



## RESEARCH ARTICLE

## A new perspective on solar dimming over the Tibetan Plateau

Changgui Lin<sup>1</sup>  | Huanping Wu<sup>2</sup> | Tinghai Ou<sup>1</sup> | Deliang Chen<sup>1,3</sup> <sup>1</sup>Regional Climate Group, Department of Earth Sciences, University of Gothenburg, Gothenburg, Sweden<sup>2</sup>National Climate Center, China Meteorological Administration, Beijing, China<sup>3</sup>Institute of Tibetan Plateau Research, Chinese Academy of Sciences, Beijing, China**Correspondence**Deliang Chen, Regional Climate Group, Department of Earth Sciences, University of Gothenburg, Box 460, SE-405 30 Gothenburg, Sweden.  
Email: deliang@gvc.gu.se**Funding information**

Strategic Priority Research Program of Chinese Academy of Sciences, Grant/Award Number: XDA20060401; Swedish Foundation for International Cooperation in Research and Higher Education, Grant/Award Number: Deliang Chen; Vetenskapsrådet, Grant/Award Number: Deliang Chen

Solar radiation changes (dimming/brightening) have recently received growing attention within the research community, although there is currently no generally accepted explanation. This article aims to provide a new perspective for identifying the reasons behind solar dimming/brightening by using long-term measurements of direct and diffuse solar radiation, unlike previous studies which have focused on global solar radiation. We postulate that extinction processes can be more readily revealed by direct and diffuse radiation measurements with the help of a modelling tool that treats the two components separately. An example is presented for Golmud and Lhasa in the northern and southern Tibetan Plateau (TP) respectively, over the period 1957–2013. The following is found: (a) ground-based observed cloud cover alone hardly explains the observed solar dimming at the two sites; (b) both the cloud-free direct radiation transmittivity ( $\tau_{dir}$ ) and diffuse radiation proportion ( $p_{dif}$ ) declined; (c) variations in  $p_{dif}$  are overwhelmingly dominated by variations in aerosols, while those in  $\tau_{dir}$  are related to variations in both aerosol and water vapour; (d) on top of the suggested reduced aerosol concentrations, decreased snow cover can partly explain declined diffuse radiation via lowered surface albedo; (e) the decline in  $\tau_{dir}$  can be partly attributed to the wetting atmosphere via strengthened absorption; and (f) the impact of volcanic eruptions was also identified from such radiative parameters, lasting into the following summer and especially strong in the southern TP.

**KEYWORDS**

direct and diffuse radiation, extinction processes, Tibetan Plateau

**1 | INTRODUCTION**

The incidence of solar radiation at the Earth's surface is of particular importance in climate system studies because it is the major source of the Earth's surface energy budget. This is especially true for the elevated Tibetan Plateau (TP). Here, low air mass amount, water vapour content, and aerosol concentration mean that the TP receives stronger incoming solar radiation than its surroundings, affecting the glacier dynamics.

Recently, growing attention has been paid to the variations in the received solar radiation and their attribution (Wild, 2012, and the references therein). Furthermore, there has been a widely reported transition of surface solar irradiance from dimming to brightening around the year 1990, observed from both ground measurements and satellite

observations in many regions of the world (e.g., Pinker *et al.*, 2005; Wild *et al.*, 2005; Wild, 2012). However, this transition did not occur over the TP. Rather, an overall declining trend has been observed from quality-controlled measurements over recent decades (Tang *et al.*, 2011). Simultaneously, there has been a decrease in total cloud cover (TCC) commonly observed at meteorological stations in China (Xia, 2010). With this paradox of changes in surface solar irradiance and TCC in China, solar dimming seems to naturally be the consequence of increasing aerosol emissions (e.g., Kaiser, 2000; Qian *et al.*, 2006), making it of interest to study.

You *et al.* (2013) related solar dimming to increasing aerosol emissions for the TP. With relatively low values of aerosol optical depth (AOD) (Xia *et al.*, 2011; Xu *et al.*, 2015), the TP is one of cleanest regions in the world and has

been less impacted by anthropogenic activities (Cong *et al.*, 2009). According to a recent quantitative estimation (Lin *et al.*, 2015), aerosol emissions accounted for approximately 20% of the typical solar dimming for the whole of China. By this token, aerosol emissions are unlikely to have played a dominant role in solar dimming over the “clean” TP. In contrast to You *et al.* (2013), Yang *et al.* (2012) linked the solar dimming to increases in deep cloud cover, associated with more water vapour in the atmosphere under surface warming.

Not limited to the TP, as yet, there is no plausible explanation for solar dimming/brightening due to the lack of long-term measurements for aerosol properties and the complexity of aerosol–cloud–radiation interaction (e.g., Wild, 2012). Moreover, most previous studies have focused on global (here referred to as broadband spectrally integrated) solar radiation (referred to as  $R_g$ ); a catch-all measurement of solar radiation that mixes different extinction processes throughout the atmosphere. Thereby, understandings of solar irradiance variations are limited.

In this article, we attempt to provide a new perspective for identifying the reasons behind solar dimming/brightening with the help of both long-term direct and diffuse solar radiation (referred to as  $R_{dir}$  and  $R_{dif}$ , respectively) observations. To advance current knowledge of solar dimming/brightening, an analysis detailing the extinction processes (i.e., scattering and absorption) is expected to reveal the roles of different the factors that impact on solar irradiance variations. As such, the availability of reflecting long-term changes in the intensity of extinction processes is presented in Section 2. Here, the intensity of scattering/absorption can be revealed from the direct radiation transmittivity ( $\tau_{dir}$ ) and the proportion of diffuse radiation ( $p_{dif}$ ); the two atmospheric parameters that are required for  $R_{dir}$  and  $R_{dif}$  modelling and can be estimated from the relevant measurements ( $R_{dir}$  and  $R_{dif}$ ) with such a modelling tool. An example for the TP is presented. Following a revisit to the association between observed solar radiation and cloud cover, detailed analyses were carried out for cloud-free conditions to explore the roles played by factors other than clouds.

In addition to the attribution of long-term changes in solar irradiance, volcanic impacts are also of interest as these affect both global and regional climate change at various timescales (e.g., Robock, 2000; Shindell *et al.*, 2004; Gleckler *et al.*, 2006; Emile-Geay *et al.*, 2008; Anchukaitis *et al.*, 2010; Sun *et al.*, 2018). Due to the lack of aerosol property observation, the volcanic impact on surface solar irradiance and its duration over a specific region (e.g., the TP) require further examination. Because cloud cover greatly affects atmospheric radiative properties, volcanic signals in surface irradiance observations are always masked. Based on the cloud-free  $\tau_{dir}$  and  $p_{dif}$  time series, this study therefore also offers a sensitive way to discuss the volcanic impact over the TP region.

## 2 | METHODOLOGY

### 2.1 | Observations and site information

Daily mean  $R_{dir}$  and  $R_{dif}$  observations were used to calculate  $\tau_{dir}$  and  $p_{dif}$  with a modelling tool that treats the two components of solar radiation separately. These observations, as well as TCC and low-level cloud cover (referred to as LCC) observed by an observer, are available at a small number of stations managed by the China Meteorological Administration (CMA).

There has been a change of instruments to measure solar radiation in China. Before 1990, the Yanishevsky thermoelectric actinometer was used for  $R_{dir}$  measurement, and the Yanishevsky thermoelectric pyranometer for measurements of global solar radiation and  $R_{dif}$ . After 1990, the DFY-3 pyrheliometer was used for  $R_{dir}$  measurement; and the DFY-4 pyranometer for measurements of global solar radiation and  $R_{dif}$ . According to Shi *et al.* (2008), who did a quality control of the radiation data collected by CMA, the data quality of global and diffuse irradiance in the TP is very good; less than 1% of erroneous and suspected data are found in the measurements, though the instrumental change may have led to potential inhomogeneity of the data records around 1990.

In this case study, two stations from the northern and southern TP, Golmud and Lhasa, were chosen because there are long-term records of  $R_{dir}$  and  $R_{dif}$  (available from 1 July, 1957 to 30 June, 2013). Figure 1 shows the location of the two stations and their surrounding topography. Golmud is located at the southern Qaidam Basin, to the north of Kunlun Mountains, and has a comparatively low elevation of 2,800 m in the shadow cast by the highlands to the south. Lhasa sits in a flat river valley with an elevation of about 3,600 m, of which the surrounding mountains have elevations up to 5,500 m.

### 2.2 | Calculation of $\tau_{dir}$ and $p_{dif}$

The observed direct and diffuse radiation were used to derive two parameters  $\tau_{dir}$  and  $p_{dif}$ , which in turn were used to study the extinction processes. Solar Analyst (Fu and Rich, 1999), an ESRI ArcView geographical information systems extension designed for direct and diffuse radiation modelling, was chosen to derive the  $\tau_{dir}$  and  $p_{dif}$  because it uses a simple transmission model with these two parameters to account for atmospheric depletion effects. The complex surrounding topography (Figure 1) may have great impact on both  $R_{dir}$  and  $R_{dif}$  received by measurement instruments. Although the topographical effect cannot affect the long-term radiation variability, we still choose Solar Analyst, which solves this effect, to realistically derive the  $\tau_{dir}$  and  $p_{dif}$  because we intend to use the model to study the impact of topography on surface radiation in another project. 500-m Digital Elevation Model (DEM) data, resampled from the USGS 30-m DEM product, was used by Solar Analyst to generate an upward-looking hemispherical viewshed



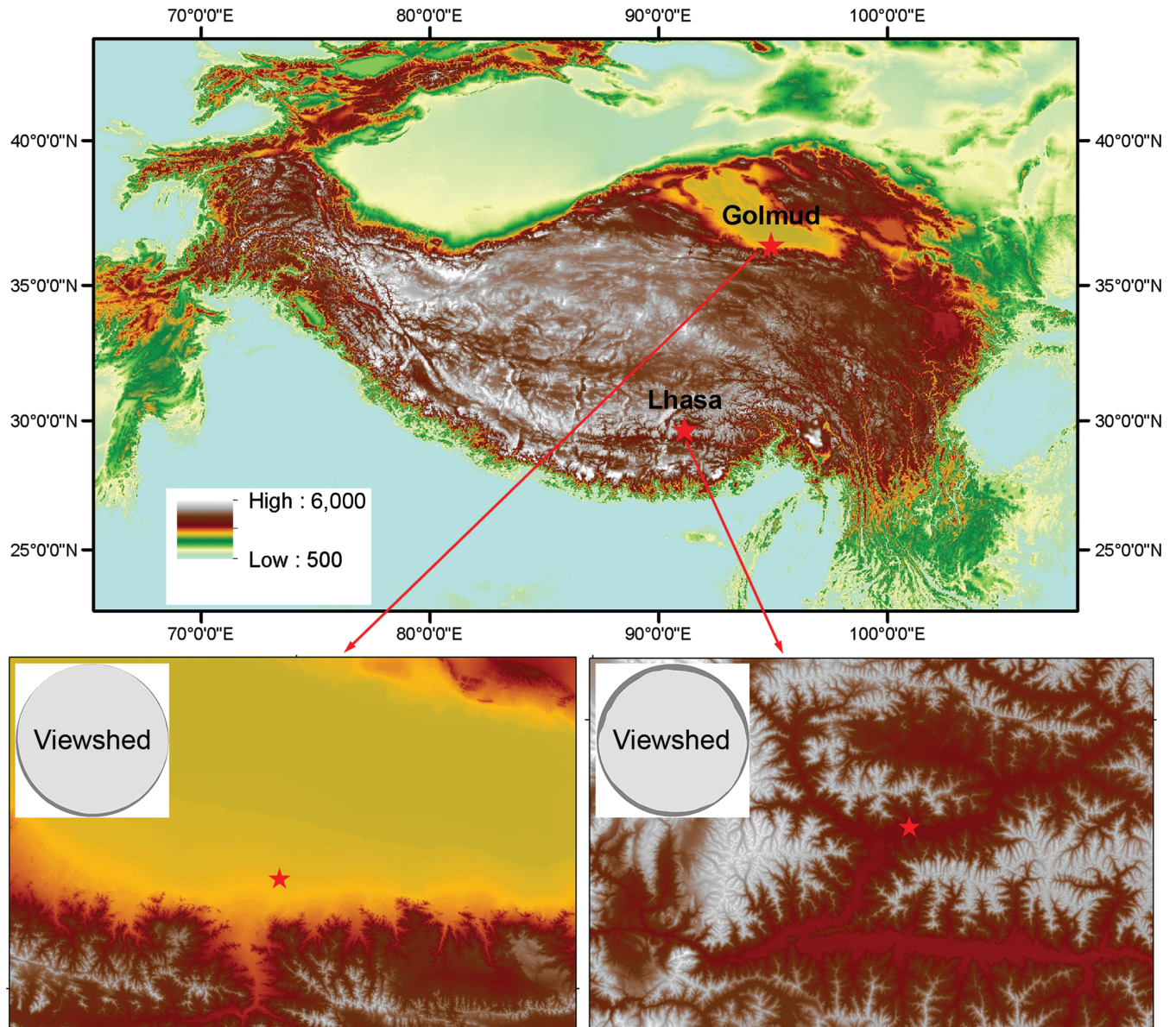


**FIGURE 1** Location, surrounding topography, and upward-looking hemispherical view shed (generated by solar analyst with dark grey as view blocked) of the two sites (Golmud and Lhasa) [Colour figure can be viewed at [wileyonlinelibrary.com](http://wileyonlinelibrary.com)]

(Figure 1), which serves to solve the topographical shadowing effect.

Considering a horizontal surface as the standard platform for radiation observation, the equations used for calculating direct and diffuse irradiance at zenith angle ( $\theta$ ) and azimuth angle ( $\alpha$ ) in Fu and Rich (1999) can be rewritten as:

$$I_{dir}(\theta, \alpha) = I_{const} \tau_0^{m(\theta, h)} f_{topo}(\theta, \alpha) \cos(\theta), \quad (1a)$$

$$I_{dif}(\theta, \alpha) = R_{glb} p_{dif} w(\theta, \alpha) f_{topo}(\theta, \alpha) \cos(\theta), \quad (1b)$$

with:

$$m(\theta, h) = \exp(-0.000118h - 1.638E - 9h^2) / \cos(\theta), \quad (1c)$$

$$R_{glb} = I_{const} \tau_0^{m(\theta_0, h)} / (1 - p_{dif}), \quad (1d)$$

where  $I_{dir}$  and  $I_{dif}$  are the estimated surface direct and diffuse irradiance, respectively;  $I_{const}$  is the solar constant

( $1,367 \text{ W m}^{-2}$ );  $\tau_0$  is the atmospheric transmittivity (averaged at all wavelengths) at sea level for the shortest path (normal to the horizontal surface);  $m$  is the relative optical path length (measured relative to the zenith path length), determined by  $\theta$  and the site elevation ( $h$ ) above sea level (using Equation 1c, for  $\theta < 4/9\pi$  and lookup tables for refraction correction at  $\theta \geq 4/9\pi$ );  $f_{topo}()$  is simply a blocking mechanism for both direct and diffuse radiation, giving values of 0 and 1 for an upward-looking view being blocked and non-blocked respectively;  $R_{glb}$  is the global normal radiation consisting of a diffuse term with the proportion of  $p_{dif}$  and a direct term with the proportion equal to  $1 - p_{dif}$ , and operationally, for a specific solar position ( $\theta = \theta_0$ ,  $\alpha = \alpha_0$ ), can be calculated by estimating the direct radiation without correction for angle of incidence and topographical shadowing effect, then correcting for the proportion of direct radiation (see Equation 1d); and  $w()$  is the weight function that

defines the density of diffuse radiation from varied  $\theta$  and  $\alpha$ , being the same from all sky directions in a uniform diffuse model, while varying with  $\theta$  in a standard diffuse model. In this study, the former diffuse model is used for cloud-free conditions and the latter for cloudy days.

The sea-level transmittivity  $\tau_0$  being corrected to the height of site elevation is then the  $\tau_{dir}$ , which can appropriately be compared with transmittivity due to atmospheric compositions, as follows:

$$\tau_{dir} = \tau_0 \exp(-0.000118h - 1.638E - 9h^2). \quad (2)$$

Daily estimated  $R_{dir}$  and  $R_{dif}$  can be calculated by integrating Equations 1a and 1b respectively, with constant  $\tau_{dir}$  and  $p_{dif}$  for each day, as follows:

$$R_{dir} = \int_{t=t_{sunrise}}^{t=t_{sunset}} I_{dir}(\theta, \alpha) dt, \quad (3a)$$

$$R_{dif} = \int_{t=t_{sunrise}}^{t=t_{sunset}} \int_{\alpha=0}^{\alpha=2\pi} \int_{\theta=0}^{\theta=\pi/2} I_{dif}(\theta, \alpha) \sin(\theta) d\theta d\alpha dt, \quad (3b)$$

where  $t_{sunrise}$  and  $t_{sunset}$  are the time of sunrise and sunset. Of note is that  $\theta$  and  $\alpha$  in Equation 3a are subject to the solar position, being varied depending upon the time and date, whereas those in Equation 3b are not.

Inserting Equations 1a–d and 2 into Equations 3a,b, we know that the  $R_{dir}$  estimation in the Solar Analyst depends only on the  $\tau_{dir}$  whereas the  $R_{dif}$  estimation depends on both the  $\tau_{dir}$  and  $p_{dif}$ . Thus, the first step is to derive  $\tau_{dir}$ . Operationally, by varying  $\tau_{dir}$  (starting from 0 with an increment of 0.0001) in the Solar Analyst, the simulated daily  $R_{dir}$  was compared with the observed. The  $\tau_{dir}$  value of each day was determined when the difference between the two is less than  $0.01 \text{ MJ m}^{-2} \text{ day}^{-1}$ . After the  $\tau_{dir}$  has been derived,  $p_{dif}$  is then the only variable unresolved in Equation 3b and a similar procedure was conducted to derive it.

### 2.3 | Atmospheric extinction processes relating to scattering and absorption

Variations in surface solar irradiance can result from changes in solar input, clouds, and the atmospheric composition (mainly aerosols, water vapour, and ozone) that attenuates atmospheric transmission due to scattering/absorption processes. We started our analyses by examining the association between cloud cover (either TCC or LCC) and solar radiation (in terms of  $R_g$ ,  $R_{dir}$ ,  $R_{dif}$  and moreover,  $\tau_{dir}$  and  $p_{dif}$ ), discussing the role played by clouds in solar dimming. Following this, the role played by atmospheric compositions under cloud-free conditions is of our special concern. The intensity of scattering/absorption is postulated to be further implicitly reflected in  $\tau_{dir}$  and  $p_{dif}$ . As a common radiation transmission model (e.g., Leckner, 1978; Yang *et al.*, 2001), transient  $I_{dir}$  and  $I_{dif}$  can be expressed as follows:

$$I_{dir} = I_{const} \cos(\theta) \tau_s \tau_a, \quad (4a)$$

$$I_{dif} = I_{const} \cos(\theta) \beta (1 - \tau_s) \tau_a, \quad (4b)$$

where  $\theta$  is subjected to the sun position,  $\tau_s$  and  $\tau_a$  are the transmittivity due to scattering and absorption respectively, and  $\beta$  is the proportion of forward scattering. Under cloud-free conditions, atmospheric extinction due to scattering consists of contribution from gaseous molecules (so-called Rayleigh scattering) and aerosol particles; the latter being more dominant in terms of both the magnitude and the variation of scattering intensity. Atmospheric absorption attenuates the incoming radiation by converting the radiation energy into excitation energy of the molecules, which is wavelength dependent, and alters the apparent spectral signature of the target. Ozone in the stratosphere absorbs about 99% of the solar ultraviolet (UV) radiation shorter than 320 nm, while water vapour mainly acts on the infrared region. In this study, we correlated  $\tau_{dir}$  and  $p_{dif}$  to these factors (aerosols, water vapour, and ozone) to explore the roles played by each of them. AOD describes the attenuation of sunlight by a column of aerosol, and thus serves as a measure of the optical properties of aerosol column concentration. Both Pearson ordinary and partial correlation coefficients were used to evaluate the association between the radiation parameters and the atmospheric composition factors considered. Long-term trends in these factors were then examined using ordinary least square regression. Instead of using trends in the contents of water vapour and ozone, trends in the transmittivities relating to water vapour absorption and ozone absorption were taken in order to be easily compared with changes in  $\tau_{dir}$  and  $p_{dif}$ . Such transmittivities can be calculated using the following equations from the hybrid solar radiation model (Yang *et al.*, 2001):

$$\tau_{PWV} = \min[1.0, 0.909 - 0.036 \ln(mw)], \quad (5a)$$

$$\tau_{TOZ} = \exp[-0.0365(ml)^{0.7136}], \quad (5b)$$

$$m = 1 / [\cos(\theta) + 0.15(183.886 - 57.296\theta)^{-1.253}], \quad (5c)$$

where  $\tau_{PWV}$  and  $\tau_{TOZ}$  are the transmittivities relating to water vapour absorption and ozone absorption, respectively;  $w$  is the precipitable water vapour (PWV) in mm;  $l$  is the total column ozone (TOZ) with unit of 100 DU; and  $m$  is the relative air mass. To make  $\tau_{PWV}$  and  $\tau_{TOZ}$  along the direction normal to horizontal surface corresponding to  $\tau_{dir}$ , the zenith angle  $\theta$  is set to 0. The significance levels (measured by  $p$  values) were tested using a Student's  $t$  distribution for a transformation of both the correlation coefficients and linear slopes.

### 2.4 | Other data sets

Satellite data retrieved from the Multiangle Imaging Spectro-Radiometer (MISR) and Moderate Resolution Imaging Spectroradiometer (MODIS), both aboard the Terra spacecraft, are available from March 2000 and have been widely used



to understand atmospheric processes (Kaufman *et al.*, 2002). MISR Level 3 daily products of AOD and absorbing AOD (AAOD) (at green band with a nominal centre wavelength of 555 nm) were chosen for analysis in view of its better performance over (semi-)arid land cover compared to MODIS retrievals (e.g., Abdou *et al.*, 2005; Prasad and Singh, 2007; Xia *et al.*, 2008). PWV derived from sounding observations, available from the Integrated Global Radiosonde Archive from the National Climatic Data Center (Durre *et al.*, 2006), is considered a good candidate for this analysis. However, most records from the pre-1991 period have been erased to meet quality control rules, and are thus not available for the long-term change analysis. For the ozone measurements, the Total Ozone Mapping Spectrometer (TOMS) instruments flown on NASA-satellites (Nimbus-7:1978–1993, Meteor-3:1991–1994, and Earth Probe: 1996–2006) provided global measurements of the daily TOZ. These, however, are likewise not appropriate for the long-term change analysis. ERA-interim (Dee *et al.*, 2011), as the latest global atmospheric reanalysis, produced by the European Centre for Medium-Range Weather Forecasts (ECMWF), provides both PWV and TOZ from 1979. Hence, this data set was chosen for the analysis. Though it is not directly observational, it assimilates available ground-based observations and satellite data including radiosonde measurements and TOMS TOZ as mentioned above. According to the assessment from Lu *et al.* (2015), ERA-interim is one of the best reanalyses to reflect the long-term trends revealed by a Bayesian approach over the TP. To derive the time series at a station from grid data, AOD is averaged from  $5 \times 5$  grids of MISR product (with a spatial resolution of  $0.5^\circ \times 0.5^\circ$ ) centered at the station, while PWV and TOZ are averaged from  $3 \times 3$  grids of ERA-interim reanalysis (with a spatial resolution of  $0.75^\circ \times 0.75^\circ$ ).

Reflected solar radiation, mainly incorporated in the observed diffuse radiation, is not considered in the Solar Analyst; however, it can be affected by changes in surface albedo and in turn contributes to observed variations in solar radiation. Weekly snow cover data from Northern Hemisphere EASE-GRID 2.0 (version 4.0; with a spatial resolution of  $25 \times 25$  km and available from 6 October, 1966 to 25 December, 2016) were used to examine long-term changes of annual occurrence frequency of weeks with snow cover identified, because snow cover changes can significantly alter the surface albedo. According to Iqbal (1983, p. 156), the equation for  $R_{dif}$  calculation with reflected radiation from the surface and backscattered can be expressed as follows:

$$R_{dif} = \frac{R_{dif, \rho_{sfc}=0}}{1 - \rho_a \rho_{sfc}}, \quad (6)$$

where  $\rho_a$  and  $\rho_{sfc}$  are the atmospheric and surface albedo, respectively, and  $R_{dif, \rho_{sfc}=0}$  is the diffuse radiation with zero  $\rho_{sfc}$ . Changes in  $\rho_a$  are negligible. Therefore, its value was

set to be constant, with a typical value of 0.2. To estimate the contribution of changes in surface albedo, we let the term  $R_{dif, \rho_{sfc}=0}$  to be constant with time. Here, we defined the relative change of  $R_{dif}$  as:

$$R'_{dif, t} = \frac{R_{dif, t} - R_{dif, t=0}}{R_{dif} \times 100\%}, \quad (7)$$

which further approximates to:

$$\begin{aligned} & \frac{R_{dif, t} - R_{dif, t=0}}{R_{dif, \rho_{sfc}=0}} \times 100\% \\ &= \left( \frac{1}{1 - 0.2\rho_{sfc, t}} - \frac{1}{1 - 0.2\rho_{sfc, t=0}} \right) \times 100\%, \end{aligned}$$

where  $t$  in the subscripts is time, and  $t = 0$  indicates the initial status. Thus, the maximum of its magnitude can be derived as follows:

$$\begin{aligned} |R'_{dif, t}| &= \frac{0.2|\rho_{sfc, t} - \rho_{sfc, t=0}|}{(1 - 0.2\rho_{sfc, t})(1 - 0.2\rho_{sfc, t=0})} \times 100\% \\ &\leq \frac{0.2|\rho_{sfc, t} - \rho_{sfc, t=0}|}{\min[(1 - 0.2\rho_{sfc, t})^2, (1 - 0.2\rho_{sfc, t=0})^2]} \times 100\% \\ &\leq \frac{0.2|\rho_{sfc, t} - \rho_{sfc, t=0}|}{(1 - 0.2\rho_{sfc, max})^2} \times 100\%. \end{aligned} \quad (8)$$

We here consider that the change in annual-mean surface albedo is equal to the change in the annual occurrence frequency of weeks with snow cover identified, by assuming an extreme situation that the surface with (without) snow cover has surface albedo equal to 1 (0). Thus, the maximum potential contribution of lowered surface albedo to solar dimming, leading to less reflected solar radiation, can be estimated using Equation 8.

## 2.5 | Analysis methods

There are some important notes of our analyses to be clarified:

The annual mean for all-sky conditions was calculated when the monthly means for all 12 months of each year were available; the monthly mean was calculated when more than 75% daily records of each month were available.

Due to limited days under cloud-free conditions, loose criteria were applied to calculate the annual mean for cloud-free conditions. The monthly mean was calculated if there is at least one record. The annual mean was then calculated only upon those calendar months of which the long-term series are with 75% coverage over the period 1957–2013, in order to avoid the contamination by seasonal variations in long-term trends. This results in annual mean series under cloud-free conditions representing wintertime (October–March) at Lhasa, where cloud-free days seldom exist in summer; this way preserves data homogeneity along the long-term series.

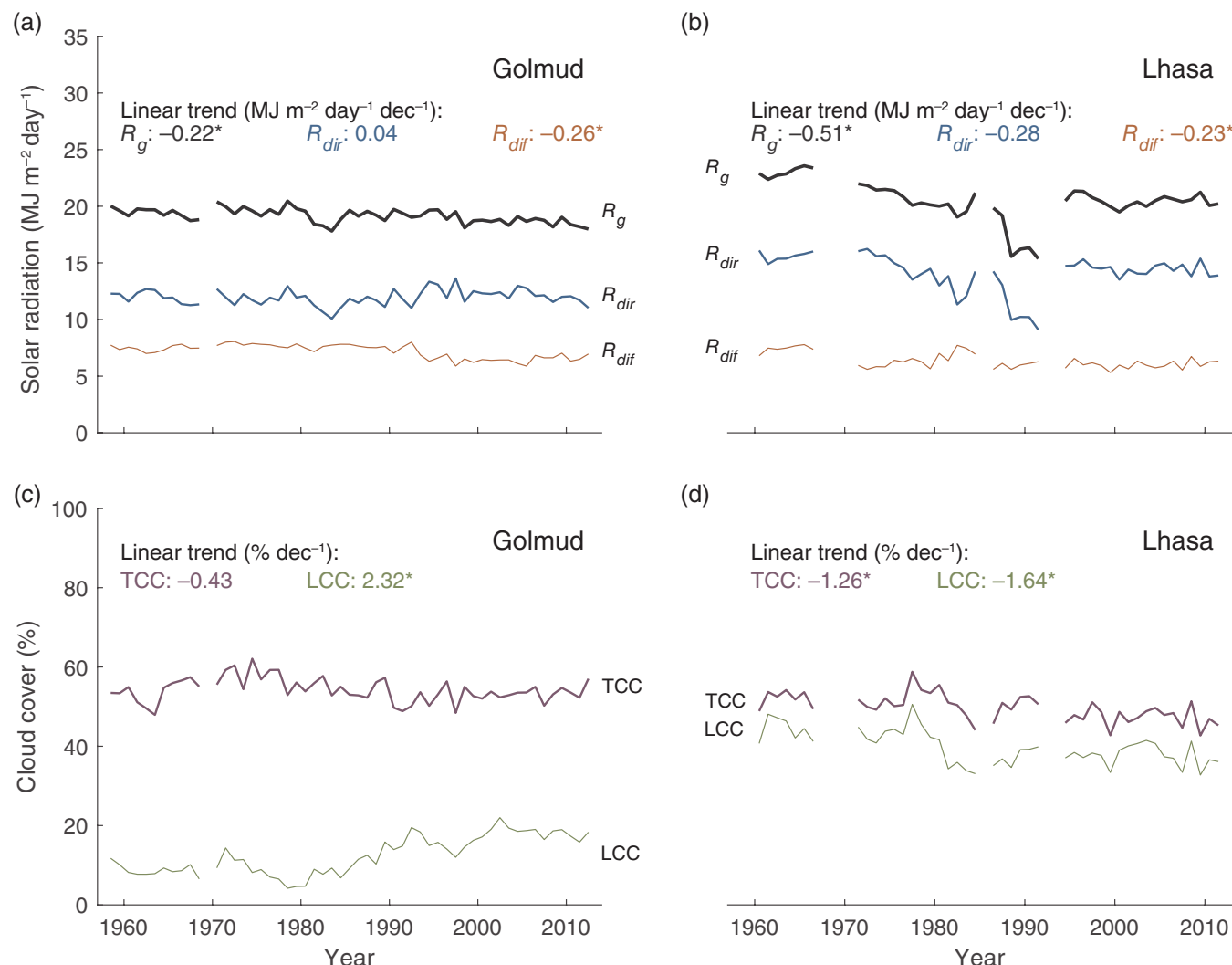


**FIGURE 2** Annual-mean time series of observed solar radiations (a, b) and cloud covers (c, d) at Golmud (a, c) and Lhasa (b, d). Value with \* denotes the linear trend being statistically significant at  $p < .05$  [Colour figure can be viewed at [wileyonlinelibrary.com](http://wileyonlinelibrary.com)]

The long-term linear trends of solar radiations were compared with causal factors to assess their contribution to the observed solar dimming. Normally, such comparisons are taken over concurrent periods where the two data sets were available. In this study, however, we compared their trends over the entire period with the available data of each parameter. This is because we noticed that there are abrupt changes in  $\tau_{dir}$  and  $p_{dif}$  around the 1980s, which can largely affect the long-term linear trend analysis over a period starting from the 1980s.

### 3 | RESULTS AND DISCUSSION

#### 3.1 | Long-term variations in observed solar radiations and clouds

The annual mean of observed solar radiations ( $R_g$ ,  $R_{dir}$ , and  $R_{dif}$ ) and cloud covers (TCC and LCC) at the two sites are presented in Figure 2. At both Golmud and Lhasa, a significant decreasing trend is observed for  $R_g$  and  $R_{dif}$ . Compared to Golmud, Lhasa has a larger loss of  $R_g$ , which is partly

attributed to the negative trend (although not statistically significant) in  $R_{dir}$ . More clouds are expected over the TP where the atmosphere gets wetter under surface warming during the last decades (Yang *et al.*, 2012; Lu *et al.*, 2015). This is therefore a candidate to explain observed solar dimming because clouds are extremely important as depletion agents of solar radiation. Regarding the selected two sites, an increasing trend is only observed for LCC at Golmud, likely to be an explanation of solar dimming there. A significant decline for both TCC and LCC at Lhasa suggests other factors to be the causes of solar dimming.

Despite the poor association between long-term trends in solar radiation and clouds, we took the analysis one step further, detailing each calendar month to explore the roles played by both TCC and LCC in solar dimming. Indeed, attention should be paid to the seasonal variation of extraterrestrial solar irradiance, which implies more depletion of solar radiation in the summertime than in the wintertime caused by the same amount of clouds; this information is not properly reflected by the above annual-mean (equally weighted upon monthly means)-based analysis. Please refer

**TABLE 1** Correlation coefficients between observed solar radiation ( $R_g$ / $R_{dir}$ / $R_{dif}$ ) and cloud cover (TCC/LCC) over the entire period for each calendar month and annual mean

	TCC			LCC		
	$R_g$	$R_{dir}$	$R_{dif}$	$R_g$	$R_{dir}$	$R_{dif}$
Golmud						
January	−.50**	−.71**	.58**	−.53**	−.30*	−.13
February	−.56**	−.66**	.52**	−.39**	−.18	−.20
March	−.70**	−.87**	.73**	−.33**	−.13	−.10
April	−.63**	−.75**	.55**	−.40**	−.12	−.26
May	−.46**	−.58**	.28*	−.51**	−.13	−.42**
June	−.49**	−.70**	.55**	−.36**	−.20	−.20
July	−.64**	−.76**	.49**	−.47**	−.27*	−.22
August	−.64**	−.75**	.42**	−.60**	−.39**	−.18
September	−.67**	−.81**	.55**	−.53**	−.24	−.29
October	−.59**	−.72**	.52**	−.66**	−.47**	−.06
November	−.29*	−.64**	.60**	−.66**	−.42**	−.08
December	−.22	−.58**	.60**	−.60**	−.34**	−.08
Annual	−.06	−.48**	.47**	−.45**	.17	−.64**
Lhasa						
January	−.42**	−.62**	.65**	−.27*	−.45**	.55**
February	−.46**	−.70**	.72**	−.20	−.44**	.64**
March	−.23	−.50**	.71**	.02	−.23	.60**
April	−.34*	−.56**	.60**	−.16	−.35*	.50**
May	−.26	−.48**	.59**	−.09	−.26	.43**
June	.00	−.27	.59**	−.06	−.28*	.46**
July	−.42**	−.70**	.69**	−.23	−.54**	.72**
August	−.36**	−.62**	.63**	−.09	−.40**	.67**
September	−.31*	−.57**	.62**	−.12	−.44**	.68**
October	−.22	−.48**	.69**	−.13	−.39**	.67**
November	−.23	−.50**	.72**	−.08	−.37**	.70**
December	−.26	−.50**	.67**	−.09	−.32*	.59**
Annual	.04	−.12	.41**	.38**	.28	.34*

\* $p < .05$ , \*\* $p < .01$ .

to Table 1 for the large difference between radiation-cloud correlation coefficients for each calendar month and annual mean. Overall, both TCC and LCC as depletion agents of  $R_g$  and  $R_{dir}$  are represented by the negative correlation coefficients (Table 1). More TCC results in more  $R_{dif}$ , as shown in the positive correlation coefficients consistently at the two sites. LCC to the  $R_{dif}$ , however, is much complex: being positively correlated at Lhasa but negatively at Golmud. This scenario is possible if increasing cloud cover at Golmud results in thicker clouds which will reflect more solar radiation to space. With regard to long-term trends, a complex situation is confronted as shown in Table 2. At Lhasa, the reduced cloud cover may, to some extent, contribute the common decline in  $R_{dif}$  via less scattering effects on incoming solar radiation; however, it fails to explain the decline in  $R_{dir}$ . The increasing LCC at Golmud, which features a strong depletion effect on incoming solar radiation, is expected to

cause decline in both  $R_{dir}$  and  $R_{dif}$ ; however, the common decline is only observed for  $R_{dif}$ .

Additional notes are made for a further discussion on the role in solar dimming played by clouds: (a) the data quality of cloud cover, of which the observation is made by different observers, is a concern especially for assessing the long-term trend; (b) the ground-based observed cloud covers can hardly provide sufficient information about cloud optical properties, which directly deal with solar extinction; and, (c) the effects of clouds on solar radiation may vary with their types, which cannot be reflected in cloud cover. For example, LCC shows a different relationship with  $R_{dif}$  at the two sites. Apart from the above notes, we indeed gain further insight into clouds' role in solar dimming by detailing our analysis into the two components of  $R_g$ . Limited by the shortage of long-term observations of cloud properties, the remaining part of this study is taken for cloud-free conditions to explore the roles played by factors other than clouds.

### 3.2 | Long-term variations in cloud-free $\tau_{dir}$ and $p_{dif}$

Figure 3 shows the daily records of  $\tau_{dir}$  and  $p_{dif}$  under cloud-free conditions at the two sites. Note that only wintertime (October–March) days were analysed for Lhasa, because cloud-free conditions seldom exist during summer monsoon seasons. For the two sites in the TP under cloud-free conditions,  $\tau_{dir}$  typically has values around 0.8 while  $p_{dif}$  0.2. Lhasa has higher  $\tau_{dir}$  yet lower  $p_{dif}$  than Golmud, meaning higher atmospheric transparency. This should be the result of the thinner tropospheric layer above Lhasa, as it has a higher elevation and comparatively lower aerosol concentrations (Xu *et al.*, 2015). Normally,  $\tau_{dir}$  is negatively correlated with  $p_{dif}$ ; that is, a higher  $\tau_{dir}$  is paired with a lower  $p_{dif}$  and vice versa. This phenomenon is indeed observed for both Golmud and Lhasa (Figure 3). The correlation coefficient between the two parameters is  $-0.88$  and  $-0.76$  for Golmud and Lhasa respectively. From Equations 4a and 4b, we can easily observe that scattering processes lead to this negative relationship; that is, stronger scattering causes more diffuse radiation but attenuates the beam radiation.

With regard to the long-term trends, however, there is an interestingly consistent negative trend for both  $\tau_{dir}$  and  $p_{dif}$  over the entire period (1957–2013) at both Golmud and Lhasa (Figure 3). In general, the decline in the two parameters indicates approximately  $1.0\%$  and  $5.7\%$   $\text{dec}^{-1}$  decreasing rate in  $R_{dir}$  and  $R_{dif}$ , respectively, for Lhasa. Meanwhile, the decreasing rate is slightly lower ( $0.6$  and  $2.4\%$   $\text{dec}^{-1}$  in  $R_{dir}$  and  $R_{dif}$ , respectively) for Golmud.

### 3.3 | Associations of $\tau_{dir}$ and $p_{dif}$ with atmospheric factors

To examine the associations of  $\tau_{dir}$  and  $p_{dif}$  with atmospheric factors (aerosols, water vapour, and ozone), their seasonal



**TABLE 2** Linear trends of observed solar radiation ( $R_g/R_{dir}/R_{dif}$ ) and cloud cover (TCC/LCC) over the entire period for each calendar month and annual mean

	Radiation			Cloud cover			
	Trend ( $\text{MJ m}^{-2} \text{ day}^{-1} \text{ dec}^{-1}$ )			Trend ( $\% \text{ dec}^{-1}$ )		Mean (%)	
	$R_g$	$R_{dir}$	$R_{dif}$	TCC	LCC	TCC	LCC
Golmud							
January	−.23**	−.04	−.20**	−1.22	1.47**	45.6	4.7
February	−.25**	−.10	−.15*	−1.27	2.61**	58.4	8.3
March	−.08	.22	−.30**	−.83	2.11**	65.3	9.6
April	−.08	.31	−.39**	−1.07	1.97**	64.4	9.3
May	−.13	.30*	−.43**	.11	2.50**	66.2	14.9
June	−.26	.11	−.37**	−.23	3.17**	66.6	23.1
July	−.25	.06	−.31**	.45	3.43**	6.7	25.4
August	−.21	.02	−.24**	−.03	3.03**	53.7	21.1
September	−.20	.08	−.28**	−.16	3.45**	54.3	17.8
October	−.27**	−.13	−.14*	.21	1.48**	41.1	7.2
November	−.22**	−.05	−.17**	−1.49	.85**	35.0	3.3
December	−.28**	−.17*	−.11	−1.05	1.31**	38.4	3.7
Annual	−.22**	.04	−.26**	−.43	2.32**	54.2	12.5
Lhasa							
January	−.50**	−.32*	−.18**	.01	−.57	25.9	19.1
February	−.37*	−.07	−.30**	−1.94*	−2.72**	39.1	3.5
March	−.46*	−.16	−.30**	−1.60*	−2.68**	52.2	41.6
April	−.38	−.13	−.25**	−1.79**	−2.42**	6.5	47.7
May	−.46*	−.35	−.10	−1.37*	−1.56*	59.6	47.6
June	−.63**	−.43*	−.20*	−1.63**	−1.71*	66.6	55.6
July	−.72**	−.51*	−.20*	−.43	−.88	78.2	64.8
August	−.54**	−.30	−.24*	−1.73*	−2.43**	79.6	66.6
September	−.51**	−.34	−.18	−1.38	−1.46*	64.4	53.9
October	−.57**	−.38*	−.19**	−.67	−.75	31.8	25.2
November	−.51**	−.36*	−.15*	−.41	−.67	19.0	13.0
December	−.43**	−.20	−.23**	−1.30*	−1.40**	18.9	12.2
Annual	−.51**	−.28	−.23**	−1.26**	−1.64**	49.7	39.8

\* $p < .05$ , \*\* $p < .01$ .

variations were examined. As shown in Figure 4,  $\tau_{dir}$  and  $p_{dif}$  exhibit sinusoidal-like seasonal change.  $\tau_{dir}$  has high values for winter while low for summer when the monsoon dominates. For  $p_{dif}$ , the opposite is true, although not completely as it has early peak values in spring but not summer (the season of valley values for  $\tau_{dir}$ ). As both of the two parameters are to a certain extent independent from the zenith and azimuth angles, the seasonal variations are largely caused by atmospheric extinction factors. Figure 5 shows that both AOD and TOZ have early peak values (May for AOD and April for TOZ), while PWV peak values appear in August as the plateau monsoon matures (Ding, 2013). According to the phase pairing, the seasonal variation of  $p_{dif}$  is, very likely, influenced by aerosols and ozone, while that of  $\tau_{dir}$  is largely influenced by water vapour.

The correlation between the radiative parameters ( $\tau_{dir}$  and  $p_{dif}$ ) and the atmospheric factors under cloud-free conditions was further investigated for the period from 2000 to

2012 because MISR AOD is only available for this period. This was achieved using both ordinary and partial linear correlation methods (Table 3). From both the ordinary and partial correlation analyses, it appears that  $p_{dif}$  is controlled by AOD because its major extinction of solar radiation is via scattering, which together with water vapour (due to its absorption processes over several bands of solar radiation) dominates  $\tau_{dir}$ 's variation. Higher correlation coefficients between  $p_{dif}$  and AOD are observed at Golmud than Lhasa (0.77 vs. 0.32 for the ordinary correlation, and 0.74 vs. 0.25 for the partial one), which is also reflected in the correlations between  $\tau_{dir}$  and AOD (0.82 vs. 0.39 for the ordinary correlation, and 0.76 vs. 0.17 for the partial one). This indicates that aerosol extinction effects are more predominant at Golmud, which is consistent with the comparatively higher AOD values at Golmud (Figure 5). Xu *et al.* (2015) also reported that AOD values in the northern TP region are higher than those in the southern part. Compared to aerosols

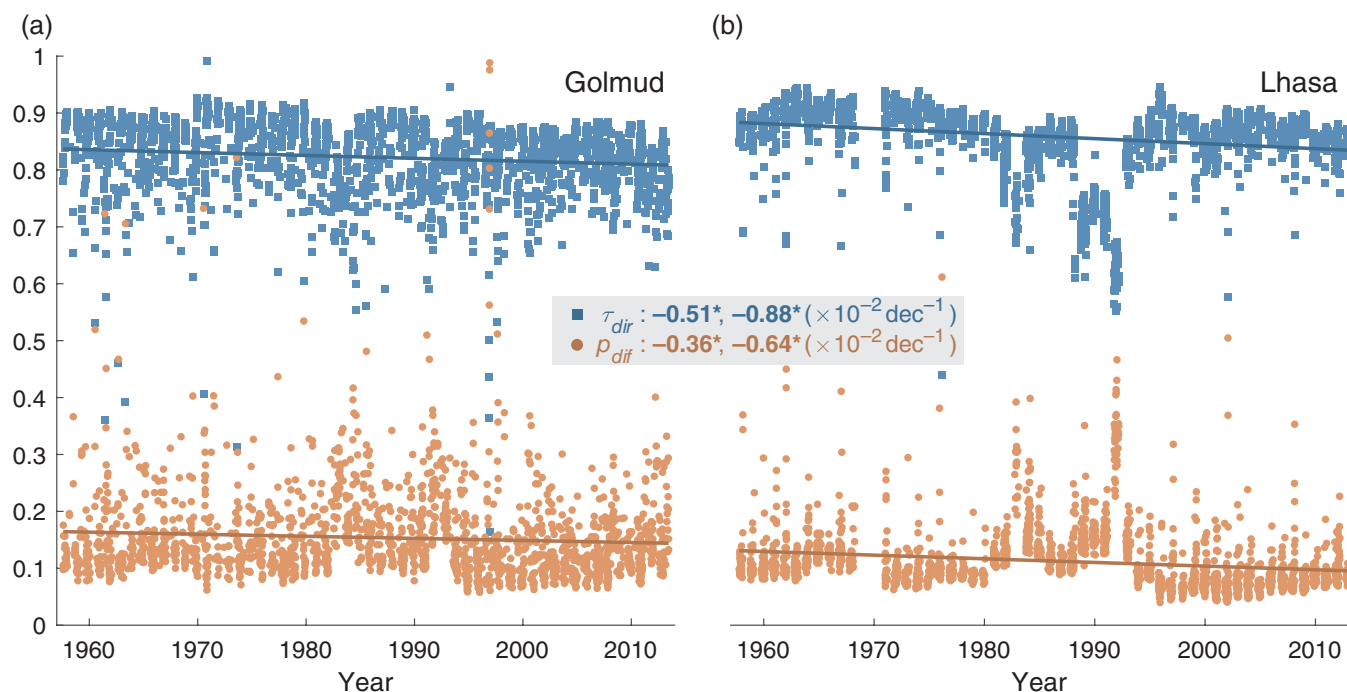


**FIGURE 3** Daily  $\tau_{dir}$  and  $p_{dif}$  under cloud-free conditions at Golmud (a) and Lhasa (b). The solid straight lines show the linear fitting, and the linear trend values (\* denotes being statistically significant at  $p < .05$ ) are given in the legend. The abrupt changes in  $\tau_{dir}$  and  $p_{dif}$  refer to volcanic emissions to be described in Section 3.5 [Colour figure can be viewed at [wileyonlinelibrary.com](http://wileyonlinelibrary.com)]

and water vapour, ozone plays a negligible role to the two radiative parameters at Golmud, while a small contribution to  $\tau_{dir}$  is observed at Lhasa. Though ozone absorbs almost 99% of the harmful UV solar radiation and plays a critical role to the Earth system and humans, it does not contribute much to global radiation variations as it functions mainly on a narrow band of solar radiation.

To evaluate the relative contribution of each factor to  $\tau_{dir}$  variations, we used the squared value of partial correlation coefficients, because the coefficients are derived after removing the effects of the other factors. At Golmud, the contribution of AOD to the variation in daily  $\tau_{dir}$  is 57.8% and that of PWV is only 6.8%; that is, AOD dominates. At Lhasa, by contrast, AOD contributes only 2.9% to the

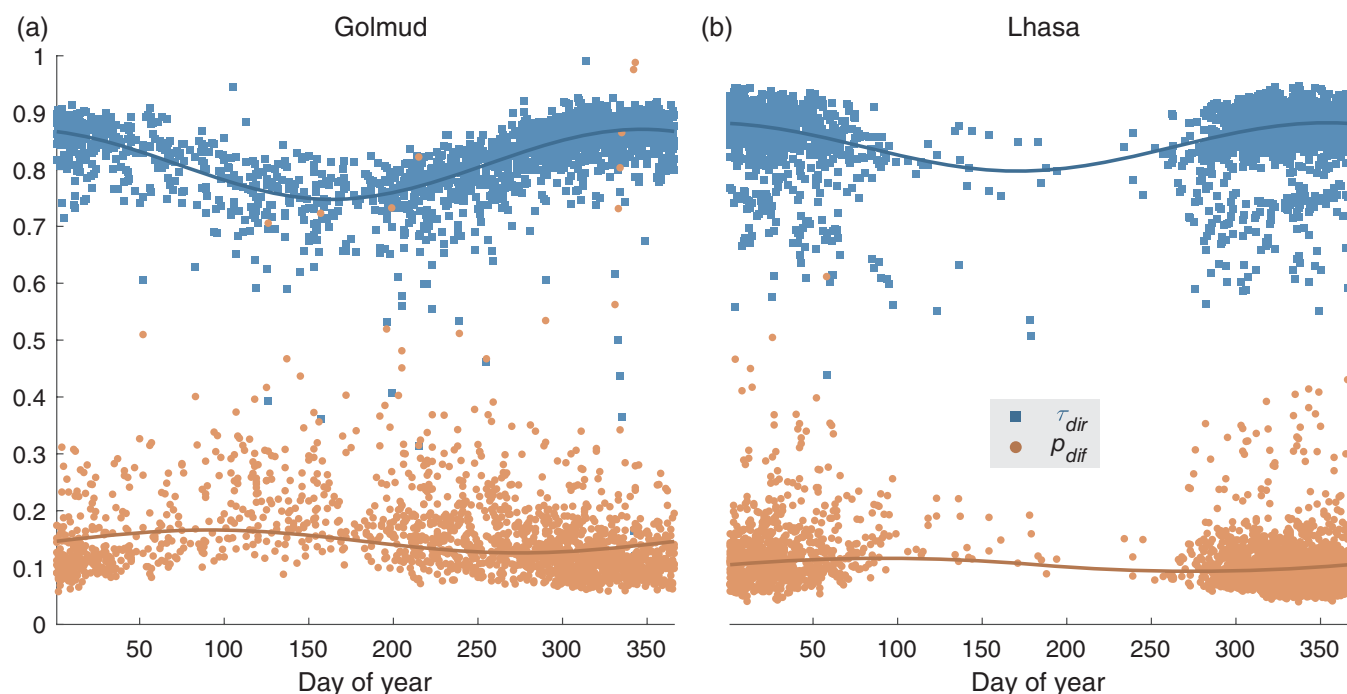


**FIGURE 4** Seasonal variation of  $\tau_{dir}$  and  $p_{dif}$  under cloud-free conditions at Golmud (a) and Lhasa (b). The solid curves show the sinusoidal fitting [Colour figure can be viewed at [wileyonlinelibrary.com](http://wileyonlinelibrary.com)]

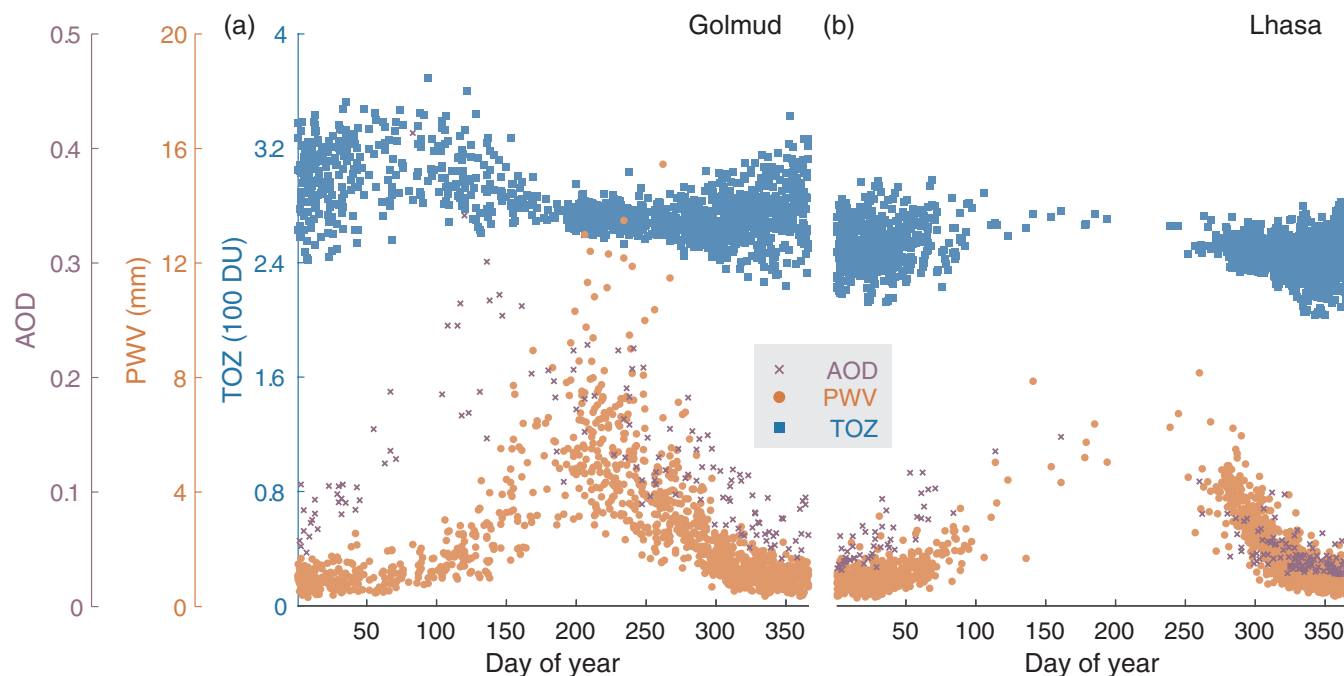


**FIGURE 5** Seasonal variation of AOD, PWV, and TOZ under cloud-free conditions at Golmud (a) and Lhasa (b) [Colour figure can be viewed at [wileyonlinelibrary.com](http://wileyonlinelibrary.com)]

variation in daily  $\tau_{dir}$ , equal to TOZ, while PWV contributes 10.2%. Comparatively, water vapour plays a more important role in the  $\tau_{dir}$  variations.

### 3.4 | Long-term trends explained by atmospheric factors

The results above show clear associations between the radiative parameters and atmospheric factors (aerosols, water vapour, and ozone). It would be interesting to explore whether the long-term trends in  $\tau_{dir}$  and  $p_{dif}$  can be explained by the long-term changes in these factors. However, due to the lack of long-term aerosol data, it is not possible to quantitatively determine the role of aerosols in these changes.

Figure 3 shows a significant decline in  $p_{dif}$  at both Golmud and Lhasa. Because reflected solar radiation, which is largely incorporated in observed  $R_{dif}$ , is not considered in the Solar Analyst, its changes affect  $p_{dif}$  values. Alongside the shrinking cryosphere (Li *et al.*, 2008), especially the retreat of glaciers (Yao *et al.*, 2012) and vegetation greening observed over the TP in response to surface warming (Shen *et al.*, 2015), the surface albedo could have been lowered, which may further result in less reflected solar radiation received by measurement instruments and in turn smaller  $p_{dif}$  values derived. As shown in Figure 6, the annual occurrence frequency of weeks with snow cover identified exhibits a significant decline at the two sites (especially Lhasa). This effect, however, is hardly quantified due to the lack of long-term, reliable data for surface albedo. A maximum of this effect was estimated based on the snow cover changes (Figure 6) and Equation 8: 13 and 22% of the decline in  $R_{dif}$

for Golmud and Lhasa, respectively, meaning a part of the negative  $p_{dif}$  trend remains unexplained.  $p_{dif}$  is largely related to the scattering processes which can be further proved from higher correlation coefficients between  $p_{dif}$  and AOD. Therefore, we suggest that aerosol concentrations, at least from the scattering aerosols, have reduced during recent decades. This is consistent with the increased visibility, a proxy of AOD (Wang *et al.*, 2009), reported by Yang *et al.* (2014) for the TP. Thus, it demonstrates that the major aerosol over the TP region is dust (Xia *et al.*, 2011; Xu *et al.*, 2015), in view of dust having a positive relationship with wind speed, which has pronouncedly declined since the 1970s (Lin *et al.*, 2013). Our results, although derived from only two stations, do not support the premise that solar dimming over the TP is caused by increasing aerosol emissions as was suggested by You *et al.* (2013).

**TABLE 3** Correlation coefficients between the daily radiative parameters ( $\tau_{dir}$  and  $p_{dif}$ ) and the atmospheric factors (AOD, PWV, and TOZ) over the period from 2000 to 2012 under cloud-free conditions

	Ordinary correlation			Partial Correlation <sup>a</sup>		
	AOD	PWV	TOZ	AOD	PWV	TOZ
Golmud						
$\tau_{dir}$	-.82***	-.49***	-.06	-.76***	-.26**	-.07
$p_{dif}$	.77***	.24**	.16	.74***	-.13	.10
Lhasa						
$\tau_{dir}$	-.39***	-.42***	-.27***	-.17*	-.32***	-.17*
$p_{dif}$	.32***	.08	.24**	.25**	-.06	.12

<sup>a</sup> Derived after controlling the other two factors. \*  $p < .05$ , \*\*  $p < .01$ , \*\*\*  $p < .001$ .



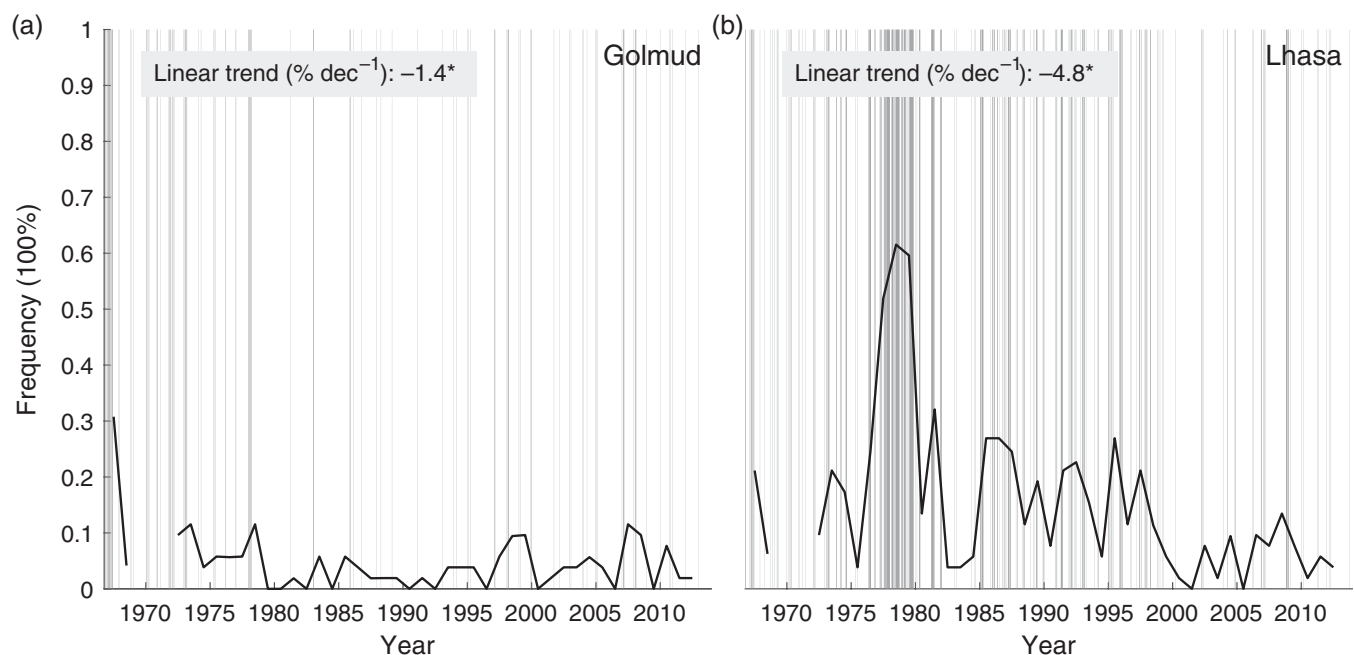


**FIGURE 6** Weeks with snow cover identified (bars) and annual occurrence frequency (solid curve) at Golmud (a) and Lhasa (b). Value with \* denotes the linear trend of annual series being statistically significant at  $p < .05$  [Colour figure can be viewed at [wileyonlinelibrary.com](#)]

Considering the decreased intensity of aerosol scattering, the decline in  $\tau_{dir}$  can largely be attributed to the strengthened absorption. As water vapour and ozone mainly dampen solar radiation through absorption, long-term trends in their corresponding transmittivity have been concentrated on. Figure 7 shows the temporal variation in the annual mean of  $\tau_{PWV}$  and  $\tau_{TOZ}$ . From 1979,  $\tau_{PWV}$  decreased with a rate of 0.11 and 0.05%  $\text{dec}^{-1}$  for Golmud and Lhasa, respectively. Thus, the wetting atmosphere over the TP (Chen *et al.*,

2015; Lu *et al.*, 2015), via strengthened absorption intensity, contributes to approximately 18 and 5% of the solar dimming at Golmud and Lhasa, respectively.  $\tau_{TOZ}$  has small degree of both the variability and long-term trend, indicating that the ozone's role is negligible. This may be explained by the small values in both the magnitude and variability of TOZ over the TP (Zou, 1996). The contributions from water vapour are more apparent compared to ozone; nevertheless, a major part of the trends in  $\tau_{dir}$  remains unexplained.

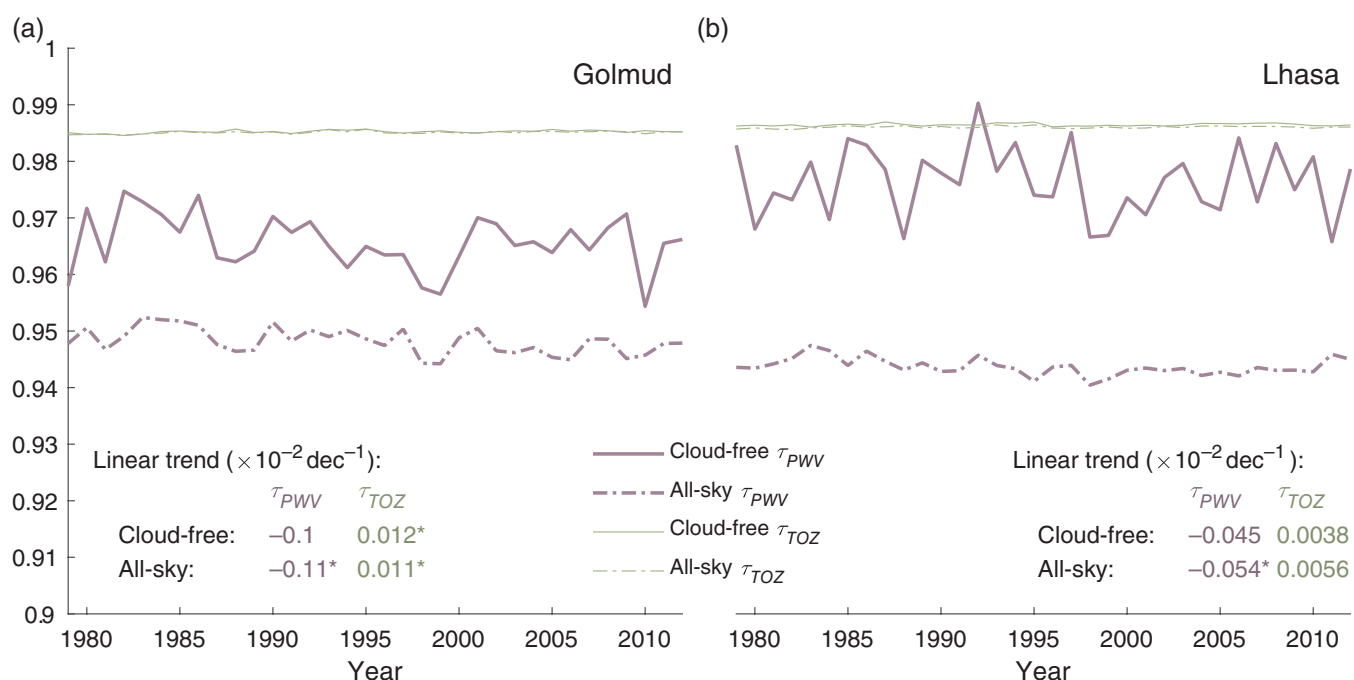


**FIGURE 7** Annual-mean time series of  $\tau_{PWV}$  and  $\tau_{TOZ}$  at Golmud (a) and Lhasa (b) from 1979–2012. Value with \* denotes the linear trend being statistically significant at  $p < .05$  [Colour figure can be viewed at [wileyonlinelibrary.com](#)]

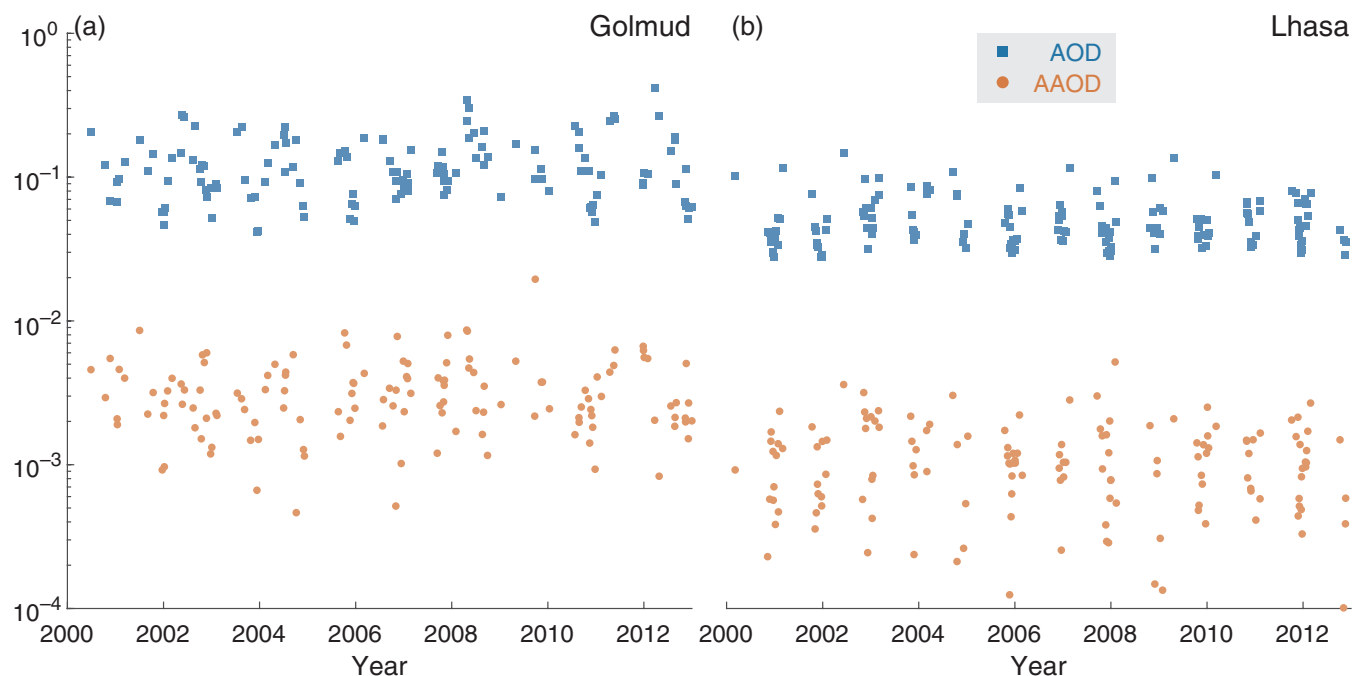


**FIGURE 8** Daily AOD and AAOD under cloud-free conditions at Golmud (a) and Lhasa (b) [Colour figure can be viewed at [wileyonlinelibrary.com](http://wileyonlinelibrary.com)]

The remaining part of the trends in  $\tau_{dir}$  may be caused by various factors. For example, an increasing concentration of black soot (absorbing aerosols) as extracted from glacier cores (Xu *et al.*, 2009) could have played a role. Note that AAOD is also available from the MISR product extracted for the two sites. However, it shows that AAOD has only about 1% of overlap with the values of AOD (Figure 8). Furthermore, emissions of both black carbon and organic

carbon, which show a very small magnitude and no trend over the TP region (Kang *et al.*, 2017, fig. 12 therein), together with Figure 8 suggest absorbing aerosols not to be a marked cause of the solar dimming.

Finally, the remaining part of the trends in  $\tau_{dir}$  unexplained addresses the need for a further study, perhaps based on quality-controlled data of both radiation and the factors.

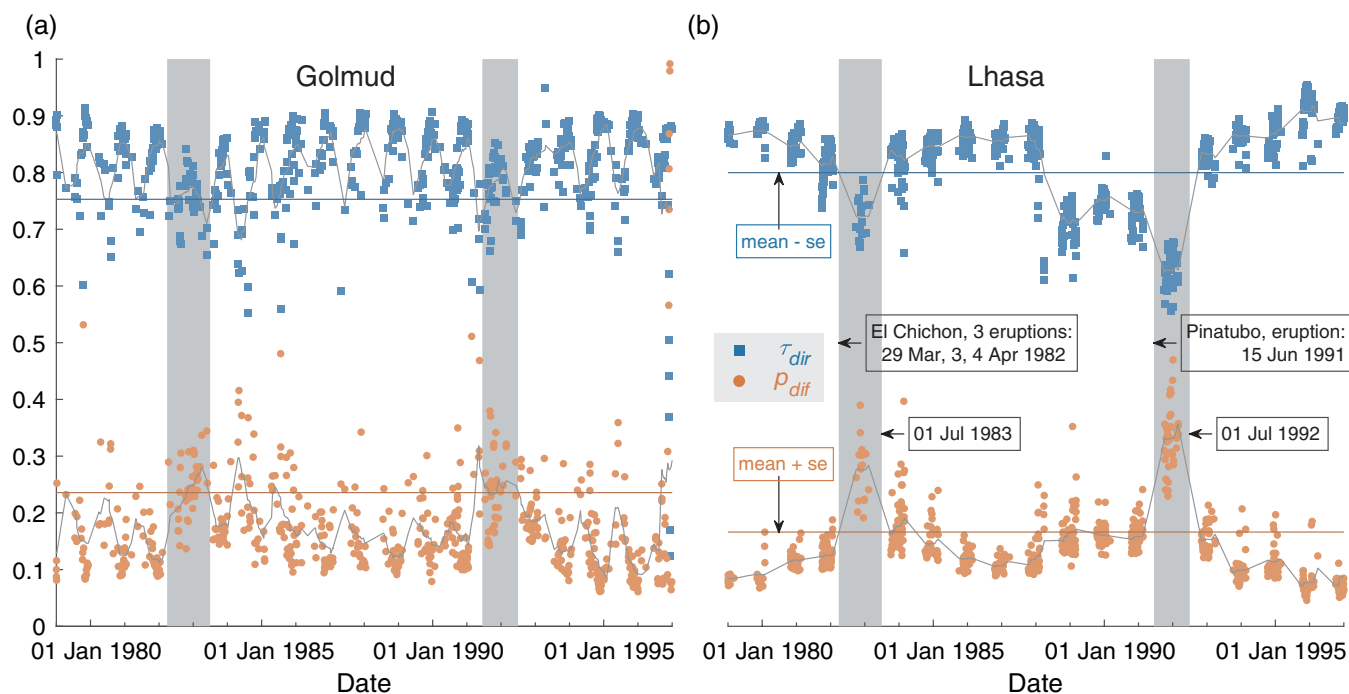


**FIGURE 9** Daily  $\tau_{dir}$  and  $p_{dif}$  (detrended) under cloud-free conditions at Golmud (a) and Lhasa (b) from 1979 to 1996. Shaded areas show the periods from the volcanic eruption days to July 1 of the following year. The straight lines show the SE below the mean of  $\tau_{dir}$  and above that of  $p_{dif}$ . The light grey curves are derived by averaging over a half-year moving window [Colour figure can be viewed at [wileyonlinelibrary.com](http://wileyonlinelibrary.com)]

### 3.5 | Volcanic impacts on $\tau_{dir}$ and $p_{dif}$

There have been two volcanic eruption events with large effects on apparent transmission during the concerned period of study (Robock, 2000, see Figure 1). One was the 1982 eruption of El Chichón volcano in Mexico. It produced three plinian eruptions (29 March, 3 April, and 4 April, 1982) with a total of 7 megatons of sulphur dioxide and 20 megatons of particulate material injecting into the stratosphere, travelling completely around the Earth within 3 weeks (Robock and Matson, 1983). An optical depth of  $\sim 0.3$  at mid visible wavelengths was measured from Chichón's cloud soon after the eruption, remaining high for several months (Patterson *et al.*, 1983). The second was the 1991 eruption of Pinatubo volcano in Philippines. As the second largest eruption of the 20th century, it injected about 17 megatons of sulphur dioxide into the stratosphere, which resulted in a global temperature drop of as much as  $-0.4^\circ\text{C}$  in the years 1991–1993 (Self *et al.*, 1996).

The daily records of  $\tau_{dir}$  and  $p_{dif}$  under cloud-free conditions for the period from 1979 to 1996 were examined, as shown in Figure 9. The abnormal values appear over the shadowed areas (period from the volcanic eruption days to 1 July, the following year). For Lhasa, the values of  $\tau_{dir}$  during the highlighted periods were below the line for mean value minus  $SE$ , while those of  $p_{dif}$  were above the line for mean value plus  $SE$ . For Golmud, this phenomenon was not so pronounced but can still be identified. This implies that the volcanic impacts can last into the summer following an eruption over the TP. From this point, the aerosols brought from the eruptions are almost erased due to convective activities and frequent precipitation events.

The impacts at Lhasa were stronger than those at Golmud. This may be because: (a) Lhasa has lower background values of AOD than Golmud according to Figure 8 and Xu *et al.* (2015); and (b) Golmud is in the westerly influenced region while Lhasa is closer to the Himalayas and strongly impacted by the Asian monsoon (Yao *et al.*, 2012); thus, there are deep convections entering the lower stratosphere which in turn introduce more stratospheric aerosols into the troposphere during summer seasons (Fu *et al.*, 2006; Lin *et al.*, 2016).

## 4 | CONCLUSIONS

This article has aimed at providing a new perspective for identifying the reasons behind solar dimming/brightening. A case study for the two sites, Golmud and Lhasa in the northern and southern TP, respectively, were presented. It reveals detailed extinction processes with help of long-term  $R_{dir}$  and  $R_{dif}$  measurements and a relevant modelling tool, thus advancing our understanding of variabilities in solar irradiance. To summarize, the case study presents multiple findings.

A significant decreasing trend is observed for all-sky  $R_g$  and  $R_{dif}$  at both Golmud and Lhasa. Cloud cover alone fails to explain the solar dimming at the two sites, suggesting other factors to be the major causes. A complex association is particularly detected between  $R_{dif}$  and LCC, which addresses that observations of other cloud properties are badly needed to further explore the roles played by clouds in solar dimming. Despite this, our analysis detailing into  $R_{dir}$  and  $R_{dif}$  reveals complex effects of TCC and LCC in the depletion of incoming solar radiation.

Both  $\tau_{dir}$  and  $p_{dif}$  under cloud-free conditions have declined during the last six decades at both Golmud and Lhasa. The decreasing rates in  $\tau_{dir}$  and  $p_{dif}$  at Lhasa are approximately 1.0 and 5.7%  $\text{dec}^{-1}$ , respectively, while Golmud has smaller decreasing rates.

The variations in daily  $p_{dif}$ , which is dominated by the scattering intensity, are overwhelmingly related to variations in aerosols. Approximately 57.8 and 6.8% (2.9 and 10.2%) of the variations in daily  $\tau_{dir}$  are explained by AOD and PWV, respectively, at Golmud (Lhasa).

Snow cover removal is observed during the past decades at the two sites. This lowers surface albedo which can further result in decreased reflected solar radiation that is embodied in measured  $R_{dif}$ . This effect contributes to no more than a quarter of the decline in  $R_{dif}$ , meaning that a large part of the negative  $p_{dif}$  trend is caused by other factors. Considering the relationship between  $p_{dif}$  and AOD, the decline of  $p_{dif}$  indicates that concentrations of the scattering aerosols have reduced over recent decades. For the long-term trend in  $\tau_{dir}$ , about 18 and 5% of the decreasing trend at Golmud and Lhasa, respectively, is explained by the wetting atmosphere.

Volcanic eruptions have large impacts on the  $\tau_{dir}$  and  $p_{dif}$  values, and the impacts are especially strong in the southern TP region. Furthermore, these impacts can last into the summer following an eruption. However, after the summer, volcanic aerosols are almost erased due to the frequent convective activities and precipitation events in summer.

Finally, it is worth mentioning that the methodology developed in this case study can be applied to any location where  $R_{dir}$  and  $R_{dif}$  measurements are available.

## ACKNOWLEDGEMENTS

The authors would like to acknowledge the National Climate Center, China Meteorological Administration (CMA) (<http://data.cma.cn/>) for providing observational data, the Earth Resources Observation and Science (EROS) Center (<https://eros.usgs.gov/>) for the USGS DEM product, the Langley Research Center Atmospheric Science Data Center (<https://eosweb.larc.nasa.gov/>) for the MISR aerosol data, the ECMWF (<https://www.ecmwf.int/>) for the ERA-interim reanalysis, and the National Snow and Ice Data Center (<http://nsidc.org/>) for the EASE-Grid 2.0 snow data (doi: <https://doi.org/10.5067/P7O0HGJLYUQU>). This work



was supported by the Strategic Priority Research Program of Chinese Academy of Sciences (XDA20060401), as well as Chinese CSC, CMA, Swedish VR, STINT, BECC, and MERGE.

## ORCID

Changgui Lin  <https://orcid.org/0000-0002-2454-5668>

Deliang Chen  <https://orcid.org/0000-0003-0288-5618>

## REFERENCES

- Abdou, W.A., Diner, D.J., Martonchik, J.V., Bruegge, C.J., Kahn, R.A., Gaitley, B.J., Crean, K.A., Remer, L.A. and Holben, B. (2005) Comparison of coincident Multiangle Imaging Spectroradiometer and Moderate Resolution Imaging Spectroradiometer aerosol optical depths over land and ocean scenes containing Aerosol Robotic Network sites. *Journal of Geophysical Research: Atmospheres*, 110(D10), D10S07.
- Anchukaitis, K.J., Buckley, B.M., Cook, E.R., Cook, B.I., D'Arrigo, R.D. and Ammann, C.M. (2010) Influence of volcanic eruptions on the climate of the Asian monsoon region. *Geophysical Research Letters*, 37(22), L22703.
- Chen, D., Xu, B., Yao, T., Guo, Z., Cui, P., Chen, F., Zhang, R., Zhang, X., Zhang, Y., Fan, J., et al. (2015) Assessment of past, present and future environmental changes on the Tibetan Plateau. *Chinese Science Bulletin*, 60(32), 3025–3035 in Chinese with English abstract.
- Cong, Z.Y., Kang, S.C., Smirnov, A. and Holben, B. (2009) Aerosol optical properties at nam co, a remote site in central Tibetan Plateau. *Atmospheric Research*, 92(1), 42–48.
- Dee, D., Uppala, S., Simmons, A., Berrisford, P., Poli, P., Kobayashi, S., Andrae, U., Balmaseda, M., Balsamo, G., Bauer, P., et al. (2011) The ERA-Interim reanalysis: configuration and performance of the data assimilation system. *Quarterly Journal of the Royal Meteorological Society*, 137(656), 553–597.
- Ding, Y. (2013) *Monsoons over China*, Vol. 16. Springer Science & Business: Media.
- Durre, I., Vose, R.S. and Wuertz, D.B. (2006) Overview of the integrated global radiosonde archive. *Journal of Climate*, 19(1), 53–68.
- Emile-Geay, J., Seager, R., Cane, M.A., Cook, E.R. and Haug, G.H. (2008) Volcanoes and ENSO over the past millennium. *Journal of Climate*, 21(13), 3134–3148.
- Fu, P. and Rich, P. M. (1999). Design and implementation of the solar analyst: an ArcView extension for modeling solar radiation at landscape scales. In *Proceedings of the Nineteenth Annual ESRI User Conference*, San Diego, USA, Vol. 1, pp. 1–31. Available at: [http://professorpaul.com/publications/fu\\_rich1999\\_esri.pdf](http://professorpaul.com/publications/fu_rich1999_esri.pdf).
- Fu, R., Hu, Y., Wright, J.S., Jiang, J.H., Dickinson, R.E., Chen, M., Filipiak, M., Read, W.G., Waters, J.W. and Wu, D.L. (2006) Short circuit of water vapor and polluted air to the global stratosphere by convective transport over the Tibetan Plateau. *Proceedings of the National Academy of Sciences*, 103(15), 5664–5669.
- Gleckler, P., Wigley, T., Santer, B., Gregory, J., AchutaRao, K. and Taylor, K. (2006) Volcanoes and climate: Krakatoa's signature persists in the ocean. *Nature*, 439(7077), 675–675.
- Iqbal, M. (1983) *An Introduction to Solar Radiation*. Vancouver: Academic.
- Kaiser, D.P. (2000) Decreasing cloudiness over China: an updated analysis examining additional variables. *Geophysical Research Letters*, 27(15), 2193–2196.
- Kang, L., Chen, S., Huang, J., Zhao, S., Ma, X., Yuan, T., Zhang, X. and Xie, T. (2017) The spatial and temporal distributions of absorbing aerosols over east asia. *Remote Sensing*, 9(10), 1050.
- Kaufman, Y.J., Tanré, D. and Boucher, O. (2002) A satellite view of aerosols in the climate system. *Nature*, 419(6903), 215–223.
- Leckner, B. (1978) The spectral distribution of solar radiation at the Earth's surface—elements of a model. *Solar Energy*, 20(2), 143–150.
- Li, X., Cheng, G., Jin, H., Kang, E., Che, T., Jin, R., Wu, L., Nan, Z., Wang, J. and Shen, Y. (2008) Cryospheric change in China. *Global and Planetary Change*, 62(3), 210–218.
- Lin, C., Yang, K., Qin, J. and Fu, R. (2013) Observed coherent trends of surface and upper-air wind speed over China since 1960. *Journal of Climate*, 26(9), 2891–2903.
- Lin, C., Yang, K., Huang, J., Tang, W., Qin, J., Niu, X., Chen, Y., Chen, D., Lu, N. and Fu, R. (2015) Impacts of wind stilling on solar radiation variability in China. *Scientific Reports*, 5, 15135.
- Lin, M., Zhang, Z., Su, L., Hill-Falkenthal, J., Priyadarshi, A., Zhang, Q., Zhang, G., Kang, S., Chan, C.-Y. and Thiemens, M.H. (2016) Resolving the impact of stratosphere-to-troposphere transport on the sulfur cycle and surface ozone over the Tibetan Plateau using a cosmogenic  $^{35}\text{S}$  tracer. *Journal of Geophysical Research: Atmospheres*, 121(1), 439–456.
- Lu, N., Trenberth, K.E., Qin, J., Yang, K. and Yao, L. (2015) Detecting long-term trends in precipitable water over the Tibetan Plateau by synthesis of station and MODIS observations. *Journal of Climate*, 28(4), 1707–1722.
- Patterson, E., Pollard, C. and Galindo, I. (1983) Optical properties of the ash from El Chichon volcano. *Geophysical Research Letters*, 10(4), 317–320.
- Pinker, R.T., Zhang, B. and Dutton, E.G. (2005) Do satellites detect trends in surface solar radiation? *Science*, 308(5723), 850–854.
- Prasad, A.K. and Singh, R.P. (2007) Comparison of MISR-MODIS aerosol optical depth over the Indo-Gangetic basin during the winter and summer seasons (2000–2005). *Remote Sensing of Environment*, 107(1), 109–119.
- Qian, Y., Kaiser, D.P., Leung, L.R. and Xu, M. (2006) More frequent cloud-free sky and less surface solar radiation in China from 1955 to 2000. *Geophysical Research Letters*, 33(1), L024586.
- Robock, A. (2000) Volcanic eruptions and climate. *Reviews of Geophysics*, 38(2), 191–219.
- Robock, A. and Matson, M. (1983) Circumglobal transport of the El Chichón volcanic dust cloud. *Science*, 221(4606), 195–197.
- Self, S., Zhao, J.-X., Holasek, R.E., Torres, R.C. and King, A.J. (1996) The atmospheric impact of the 1991 mount Pinatubo eruption. In: Newhall, C.G. and Punongbayan, R.S. (Eds.) *Fire and Mud: The Eruptions and Lahars of Mount Pinatubo, Philippines*. Seattle: University of Washington Press, pp. 1089–1116.
- Shen, M., Piao, S., Jeong, S.-J., Zhou, L., Zeng, Z., Ciais, P., Chen, D., Huang, M., Jin, C.-S., Li, L.Z., et al. (2015) Evaporative cooling over the Tibetan Plateau induced by vegetation growth. *Proceedings of the National Academy of Sciences*, 112(30), 9299–9304.
- Shi, G.-Y., Hayasaka, T., Ohmura, A., Chen, Z.-H., Wang, B., Zhao, J.-Q., Che, H.-Z. and Xu, L. (2008) Data quality assessment and the long-term trend of ground solar radiation in China. *Journal of applied meteorology and climatology*, 47(4), 1006–1016.
- Shindell, D.T., Schmidt, G.A., Mann, M.E. and Faluvegi, G. (2004) Dynamic winter climate response to large tropical volcanic eruptions since 1600. *Journal of Geophysical Research: Atmospheres*, 109(D5), D05104.
- Sun, W., Liu, J., Wang, B., Chen, D., Liu, F., Wang, Z., Ning, L. and Chen, M. (2018) A “la niña-like” state occurring in the second year after large tropical volcanic eruptions during the past 1500 years. *Climate Dynamics*, 1–15. <https://doi.org/10.1007/s00382-018-4163-x>.
- Tang, W., Yang, K., Qin, J., Cheng, C.C.K. and He, J. (2011) Solar radiation trend across China in recent decades: a revisit with quality-controlled data. *Atmospheric Chemistry and Physics*, 11(1), 393–406.
- Wang, K., Dickinson, R.E. and Liang, S. (2009) Clear sky visibility has decreased over land globally from 1973 to 2007. *Science*, 323(5920), 1468–1470.
- Wild, M. (2012) Enlightening global dimming and brightening. *Bulletin of the American Meteorological Society*, 93(1), 27–37.
- Wild, M., Gilgen, H., Roesch, A., Ohmura, A., Long, C.N., Dutton, E.G., Forgan, B., Kallis, A., Russak, V. and Tsvetkov, A. (2005) From dimming to brightening: decadal changes in solar radiation at Earth's surface. *Science*, 308(5723), 847–850.
- Xia, X.G. (2010) Spatiotemporal changes in sunshine duration and cloud amount as well as their relationship in China during 1954–2005. *Journal of Geophysical Research: Atmospheres*, 115, D00K06.
- Xia, X., Wang, P., Wang, Y., Li, Z., Xin, J., Liu, J. and Chen, H. (2008) Aerosol optical depth over the Tibetan Plateau and its relation to aerosols over the Taklimakan Desert. *Geophysical Research Letters*, 35(16), L16804.
- Xia, X.G., Zong, X.M., Cong, Z.Y., Chen, H.B., Kang, S.C. and Wang, P.C. (2011) Baseline continental aerosol over the central Tibetan plateau and a case study of aerosol transport from South Asia. *Atmospheric Environment*, 45(39), 7370–7378.

- Xu, B., Cao, J., Hansen, J., Yao, T., Joswila, D.R., Wang, N., Wu, G., Wang, M., Zhao, H., Yang, W., Liu, X. and He, J. (2009) Black soot and the survival of Tibetan glaciers. *Proceedings of the National Academy of Sciences*, 106(52), 22114–22118.
- Xu, C., Ma, Y.M., You, C. and Zhu, Z.K. (2015) The regional distribution characteristics of aerosol optical depth over the Tibetan Plateau. *Atmospheric Chemistry and Physics*, 15(20), 12065–12078.
- Yang, K., Huang, G.W. and Tamai, N. (2001) A hybrid model for estimating global solar radiation. *Solar Energy*, 70(1), 13–22.
- Yang, K., Ding, B., Qin, J., Tang, W., Lu, N. and Lin, C. (2012) Can aerosol loading explain the solar dimming over the Tibetan Plateau? *Geophysical Research Letters*, 39(20), L20710.
- Yang, K., Wu, H., Qin, J., Lin, C., Tang, W. and Chen, Y. (2014) Recent climate changes over the Tibetan Plateau and their impacts on energy and water cycle: a review. *Global and Planetary Change*, 112, 79–91.
- Yao, T., Thompson, L., Yang, W., Yu, W., Gao, Y., Guo, X., Yang, X., Duan, K., Zhao, H., Xu, B., Pu, J., Lu, A., Xiang, Y., Kattel, D.B. and Joswiak, D. (2012) Different glacier status with atmospheric circulations in Tibetan Plateau and surroundings. *Nature Climate Change*, 2(9), 663–667.
- You, Q.L., Sanchez-Lorenzo, A., Wild, M., Folini, D., Fraedrich, K., Ren, G.Y. and Kang, S.C. (2013) Decadal variation of surface solar radiation in the Tibetan Plateau from observations, reanalysis and model simulations. *Climate Dynamics*, 40(7–8), 2073–2086.
- Zou, H. (1996) Seasonal variation and trends of TOMS ozone over Tibet. *Geophysical Research Letters*, 23(9), 1029–1032.

**How to cite this article:** Lin C, Wu H, Ou T, Chen D. A new perspective on solar dimming over the Tibetan Plateau. *Int J Climatol*. 2019;39:302–316. <https://doi.org/10.1002/joc.5807>